8.6 DISPLACEMENT CASCADE SIMULATION IN TUNGSTEN AT 1025 K — W. Setyawan, G. Nandipati, K. Roche, H. Heinisch, R. J. Kurtz, (Pacific Northwest National Laboratory); and B. D. Wirth (University of Tennessee, Knoxville)

OBJECTIVE

The objective of this research is to support the prediction of irradiation damage properties of bulk tungsten-based materials using computational methods.

SUMMARY

Molecular dynamics simulation was employed to investigate the irradiation damage properties of bulk tungsten at 1025 K (0.25 melting temperature). A comprehensive data set of primary cascade damage was generated up to primary knock-on atom (PKA) energies 100 keV. The dependence of the number of surviving Frenkel pairs (N_{FP}) on the PKA energy (E) exhibits three different characteristic domains presumably related to the different cascade morphologies that form. The low-energy regime < 0.2 keV is characterized by a hit-or-miss type of Frenkel pair (FP) production near the displacement threshold energy of 128 eV. The middle regime 0.3 – 30 keV exhibits a sublinear dependence of log(N_{FP}) vs log(E) associated with compact cascade morphology with a slope of 0.73. Above 30 keV, the cascade morphology consists of complex branches or interconnected damage regions. In this extended morphology, large interstitial clusters form from superposition of interstitials from nearby damage regions. Strong clustering above 30 keV results in a superlinear dependence of log(N_{FP}) vs log(E) with a slope of 1.365. At 100 keV, an interstitial cluster of size 92 and a vacancy cluster of size 114 were observed.

PROGRESS AND STATUS

Introduction

Tungsten is considered as the primary solid material choice for divertor components in future fusion reactors due to its low sputtering coefficient, excellent thermal conductivity, relatively low neutron activation and good mechanical strength. Bulk tungsten will be exposed to energetic neutrons escaping the plasma. The deuterium-tritium reaction will produce He, through nuclear transmutation reactions, and neutrons with characteristic kinetic energies of 3.5 and 14.1 MeV, respectively. Collisions of 14.1-MeV neutrons with W atoms produce W primary-knock-on atoms (PKAs) with various recoil velocities. The spectrum of the recoil atoms as a function of recoil speed decreases drastically above ~250 keV. The purpose of the current work is to generate a comprehensive data set of the cascade damage in pure W produced by PKA up to 100 keV in particular at a temperature of interest ~1025 K.

Simulation details

The molecular dynamics (MD) technique was employed to simulate displacement cascades. For the W-W interaction, the Finnis-Sinclair type potential developed by Ackland and Thetford [1] was taken, in which the short-range part was then modified to harden the repulsion [2]. Modification was also done at distances relevant to self-interstitial configurations to improve defect formation energies. The simulations were performed using LAMMPS software [3]. Before a displacement cascade was initiated, the system was thermalized in the *NPT* ensemble for 50 ps with a Nosé-Hoover thermostat to generate a canonical distribution of velocities at 1025 K. A random PKA was then chosen and assigned an initial velocity with a random

direction. Periodic boundary conditions were applied in all axis coordinates. During the simulation, interstitials may cross the simulation cell boundary. While this does not create any issue for counting point defects, it raises a challenge when clusters of point defects need to be recognized and when spatial distribution of the clusters is important for example if the data will be embedded in a larger cell in kinetic Monte Carlo simulations. Therefore, the MD run was discarded when boundary crossing occurred. To minimize the wasted simulations, the PKA was randomly chosen from a region near the center of the cell and a large enough cell was used. All cascades generated in this work have interstitials contained in the cell throughout the simulation without crossing the boundary. At the beginning the collision cascade simulation was performed in the *NVE* ensemble using an adaptive time step allowing a maximum atom displacement of 0.005 Å per step. Cascade events and cooling were followed for ~10 ps, afterwards the system was thermalized to a target temperature in *NVT* and defect migration was followed for a total simulation time of 55 to 60 ps.

Results

The calculated melting temperature T_m using the empirical potential is 4100 ± 50 K [2], compared to experimental value of 3695 K. Hence, 1025 K represents $0.25T_m$ of the potential which is equivalent to an experimental value of ~924 K. The average displacement threshold energy E_t was calculated to be 128 eV with a minimum E_t of 48 eV [2]. Table 1 shows the size of simulation cell as a function of PKA energy ranging from below the average E_t up to 100 keV.

Vacancies (V) and interstitials (I) were determined using Wigner-Seitz cell occupancy. The number of surviving Frenkel pairs (N_{FP}) is plotted in Figure 1. The data points were averaged from 15 to 40 simulations as presented in Table 1. The plot in a log-log scale reveals three regions that can be fit with linear functions exhibiting different slopes. The lines in Figure 1 represent the least-square linear fits of the three domains namely 0.1 – 0.2, 0.3 – 30 and 30 – 100 keV that were determined on a log-log scale. The fitted equations correspond to $N_{FP} = 0.640E_{MD}^{0.334}$, $N_{FP} = 1.795E_{MD}^{0.730}$ and $N_{FP} = 0.209E_{MD}^{1.365}$ respectively where E_{MD} is given in keV. The exponents may change slightly if different fitting boundaries were used. However, the change will not eliminate the fact that the slope in the middle regime is sublinear while that in the high region is superlinear. These characteristic slopes signify a departure from the standard Norgett-Robinson-Torrens (NRT) model which predicts $N_{FP} = 0.4E_{MD}/E_t$. In the low-energy region, one may argue that the low and middle regions can be fitted as a single curve. However, the separation of the low region has a physical significance. It is related to the maximum E_t. When E_{MD} is less than the maximum E_t, the event of creating a stable Frenkel pair is a hit-or-miss process. This kind of process can result in an N_{FP} curve that has a different temperature dependence as compared to that at E_{MD} > maximum E_t. This is because at PKA energies near E_t, increasing temperature decreases the probability of easy replacement events, but, conversely, increased mobility of the temporary interstitial may increase the chance to escape the vacancy created by the PKA or the chance for the vacancy to be occupied by the **Table** surrounding lattice atoms.

1. Simulation cell size as a function of PKA kinetic energy E_{MD}. Cubic cells were used with side length L given in units of the W lattice constant a = 3.17 Å.

E_{MD} (keV)	L (a)	#atoms	#simulations
0.1, 0.15, 0.2, 0.3	15	6,750	40
0.5, 0.75	20	16,000	20
1, 1.5, 2, 3	30	54,000	20
5, 7.5	40	128,000	20
10, 15	50	250,000	15
20, 30, 40	64	524,288	15
50, 60	80	1,024,000	15
75	100	2,000,000	15
100	120	3,456,000	20

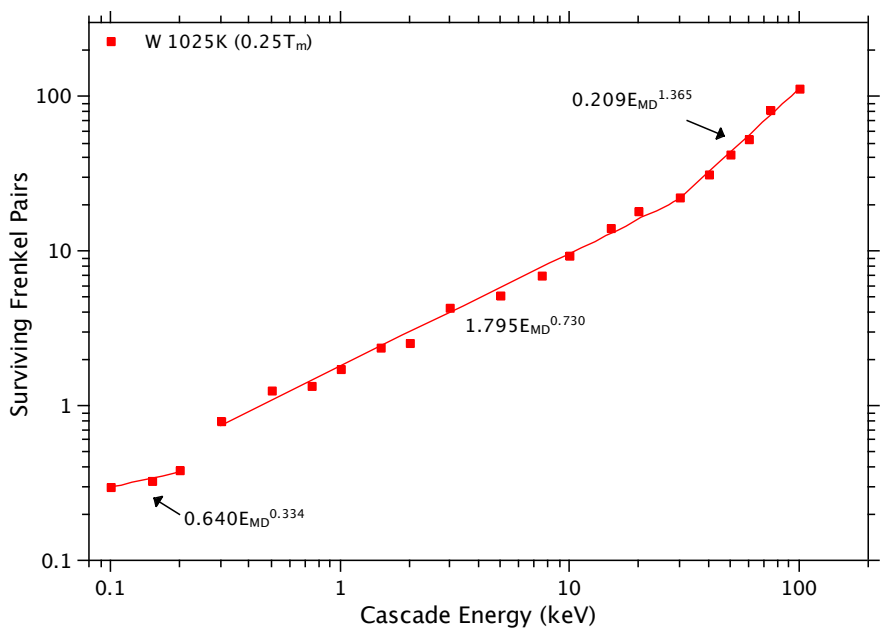

Figure 1. Characteristic curve of the number of surviving Frenkel pairs in tungsten at 1025 K (0.25 melting temperature) as a function of primary-knock-on atom kinetic energy E_{MD}. Straight lines represent least-square linear fits on a log-log scale with E_{MD} in keV.

The characteristic slopes shown in Figure 1 are presumably related to different cascade morphologies as a function of PKA energy. Snapshots of temporary vacancies and interstitials from several typical simulations with a 10-keV PKA are shown in Figure 2a. The snapshots were taken after ~0.4 ps when the maximum damage occurred. The morphology consists of a single and compact damage region. Evolution of cascade morphology from a typical simulation with 100-keV is shown in Figure 2b. In this regime, the morphology consists of complex branches or interconnected damage regions. We refer to this as an extended morphology. When a PKA

creates an extended morphology, interstitials are concentrated in the interconnecting regions between the vacancy-concentrated regions. The interstitial pockets produce large interstitial clusters at the end of simulation. It appears that the formation of large interstitial clusters and vacancy clusters mediated by the formation of an extended morphology results in the superlinear behavior of the N_{FP} curve.

Clustering of point defects was analyzed using a cutoff distance of 3.82 Å corresponding to a midpoint between the first and second nearest-neighbor distance in bcc W. Several statistical quantities were computed: dumbbell (or mono-vacancy) fraction, average cluster size <size>, maximum cluster size $size_{max}$, average of maximum cluster size $<size_{max}>$ and the ratio of $<size_{max}>/<size>$. The results are presented in Table 2. The clustering trend is evident from the decreasing dumbbell or mono-vacancy fraction and from the increasing ratio of $<size_{max}>/<size>$ as PKA energy increases. In Table 2, the PKA energy of 30 keV corresponds to the approximate location of the inflection point in the N_{FP} curve separating the region of compact and extended cascade morphology (see Figure 1). This energy is ~234 times E_t. From Table 2, one can see that the maximum size of interstitial and also vacancy clusters below 30 keV is less than 10 particles. However, above 30 keV, this value rapidly grows. This indicates strong clustering associated with the extended nature of the cascade morphology as previously discussed.

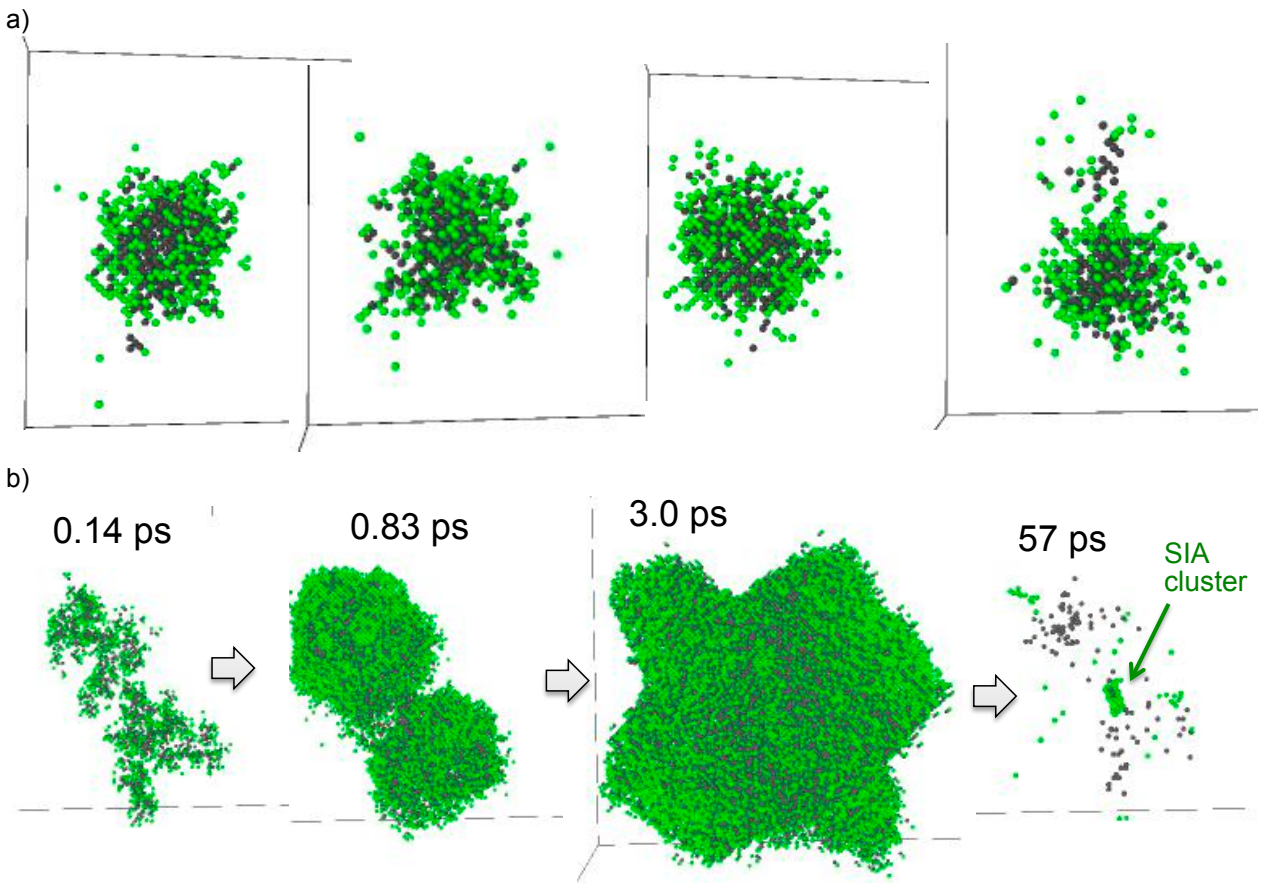

Figure 2. (a) Snaphots of temporary vacancies (black) and interstitials (green) from four different simulations with 10-keV PKA after ~0.4 ps showing a compact cascade morphology. (b) Evolution of cascade morphology from a typical run with 100-keV PKA. showing an extended morphology.

Table 2. Statistics of interstitial cluster and vacancy cluster. <> denotes the average over simulation runs.

	Interstitial clusters					Vacancy clusters				
E_{MD} (keV)	Dumbbell fraction	<size>	$size_{max}$	$<size_{max}>$	$<size_{max}>/<size>$	Monovac fraction	<size>	$size_{max}$	$<size_{max}>$	$<size_{max}>/<size>$
1	1.00	1.00	1	1.00	1.00	0.67	1.32	3	1.42	1.08
1.5	0.96	1.05	3	1.11	1.05	0.74	1.16	4	1.47	1.27
2	0.98	1.00	2	1.05	1.05	0.70	1.16	2	1.42	1.23
3	0.88	1.25	3	1.50	1.20	0.68	1.15	2	1.70	1.48
5	0.97	1.10	2	1.20	1.09	0.75	1.05	3	1.65	1.57
7.5	0.87	1.30	4	1.65	1.27	0.80	1.15	3	1.70	1.48
10	0.96	1.13	3	1.33	1.18	0.78	1.13	3	1.87	1.65
15	0.76	1.73	8	3.13	1.81	0.70	1.20	6	2.20	1.83
20	0.78	1.67	7	2.87	1.72	0.69	1.47	5	2.60	1.77
30	0.68	2.13	9	4.00	1.88	0.69	1.33	3	2.33	1.75
40	0.63	3.87	23	8.20	2.12	0.73	1.80	10	3.67	2.04
50	0.58	4.73	35	12.13	2.56	0.57	2.53	18	5.93	2.34
60	0.48	6.07	42	16.40	2.70	0.65	3.00	41	7.33	2.44
75	0.48	7.93	74	23.0	2.90	0.51	8.07	117	24.93	3.09
100	0.41	10.35	92	36.80	3.56	0.50	9.8	114	35.5	3.62

ACKNOWLEDGEMENT

Computations were performed partly on Olympus supercomputer (FUSION account) at Pacific Northwest National.

REFERENCES

[1] G. J. Ackland and T. Thetford, *Phil. Mag. A* **56** (1987) 15.
[2] N. Juslin and B. D. Wirth, *J. Nucl. Mater.* **432** (2013) 61.
[3] S. Plimpton, *J. Comp. Phys.* **117** (1995) 1.